



UNIVERSITÀ POLITECNICA DELLE MARCHE
Repository ISTITUZIONALE

Experimental study on a Savonius wind rotor for street lighting systems

This is the peer reviewed version of the following article:

Original

Experimental study on a Savonius wind rotor for street lighting systems / Ricci, Renato; Romagnoli, Roberto; Montelpare, Sergio; Vitali, Daniele. - In: APPLIED ENERGY. - ISSN 0306-2619. - ELETTRONICO. - 161:(2015), pp. 143-152. [10.1016/j.apenergy.2015.10.012]

Availability:

This version is available at: 11566/228151 since: 2022-05-25T18:19:37Z

Publisher:

Published

DOI:10.1016/j.apenergy.2015.10.012

Terms of use:

The terms and conditions for the reuse of this version of the manuscript are specified in the publishing policy. The use of copyrighted works requires the consent of the rights' holder (author or publisher). Works made available under a Creative Commons license or a Publisher's custom-made license can be used according to the terms and conditions contained therein. See editor's website for further information and terms and conditions.

This item was downloaded from IRIS Università Politecnica delle Marche (<https://iris.univpm.it>). When citing, please refer to the published version.

(Article begins on next page)

Experimental study on a Savonius wind rotor for street lighting systems

R. Ricci , R Romagnoli , , S. Montelpare , D. Vitali

This is an accepted manuscript of the following article, published on publication in Applied Energy: S. Montelpare, R. Ricci , R Romagnoli , , S. Montelpare , D. Vitali (2016) Experimental study on a Savonius wind rotor for street lighting systems. Applied Energy, Volume 161, 1 January 2016, Pages 143-152, <https://doi.org/10.1016/j.apenergy.2015.10.012>. It is deposited under the terms of Creative Commons Attribution-NonCommercial-NoDerivatives License, which permits non-commercial re-use, distribution and reproduction in any medium. The provided original work is properly cited, and it is not altered, transformed or built upon in any way.

Original work available at:

<https://doi.org/10.1016/j.apenergy.2015.10.012>

Experimental study on a Savonius wind rotor for street lighting systems[☆]

Renato Ricci^a, Roberto Romagnoli^{a,*}, Sergio Montelpare^b, Daniele Vitali^a

^a*Department of Industrial Engineering and Mathematical Sciences (DIISM)
Polytechnic University of Marche, via Breccie Bianche 1, 60131 Ancona (Italy)*

^b*Department of Engineering and Geology (INGEO), University of Chieti-Pescara, viale Pindaro 42, Pescara (Italy)*

Abstract

1 This paper investigates the aerodynamic performance of a Savonius vertical axis wind rotor to be used in
2 an innovative lamp post. The wind generator is the main part of a public lighting system (a street lamp)
3 powered by both Aeolian and Solar renewable energy sources. This study is aimed to analyze the effects of
4 different constructive solutions on the rotor performance. Experimental dynamic tests were performed on a
5 1:1 rotor model in the Environmental Wind Tunnel (EWT) of Polytechnic University of Marche (UNIVPM);
6 tests were performed at different wind velocities and for several combinations. Obtained results confirmed
7 that, in the tested range $2 - 3.3 \times 10^5$, the rotor performance do not depend on Reynolds number. Tests
8 also show that end plates and blades overlap increase the $C_{P,max}$, while external grids and structural posts
9 have negative effects on the rotor performance. Best results were obtained for a configuration having an
10 helical rotor with a $105^\circ/m$ twist, open blades overlap and end plates.

Keywords: wind tunnel, experimental measurements, Savonius rotor, wind energy, street lamp, renewable energies

11 1. Introduction

12 Last decades were characterized by a growing interest on environmental issues and consequently on
13 energy topics. Several researchers have dedicated their attention to study alternative energy production
14 sources; i.e. the use of renewable energies and smart energy production systems can effectively contribute
15 to reduce environmental impacts. Following this line, a smart lamppost, powered by renewable energy
16 sources, was developed at University "Politecnica delle Marche" (UNIVPM): the basic idea was to develop
17 a system to be used in urban environments in network or standalone configurations. The proposed street
18 light is powered by both solar and wind energies: the former is supplied by a photovoltaic panel placed
19 on the upper end of the lamppost, the latter by three vertical axis wind rotors (VAWT) inserted, in line,

[☆]This document is a collaborative effort.

*Corresponding Author

Email addresses: ricci@univpm.it (Renato Ricci), r.romagnoli@univpm.it; roberto.r73@gmail.com (Roberto Romagnoli), s.montelpare@unich.it (Sergio Montelpare), d.vitali@univpm.it (Daniele Vitali)

Nomenclature

A	rotor swept area [m^2]	s	buckets spacing distance [m]
A_t	total frontal area (rotor + frame) [m^2]	S	test section area [m^2]
a	buckets overlap distance [m]	T	torque [Nm]
c	bucket chord [m]	v_∞	free stream velocity [ms^{-1}]
C_P	power coefficient	v	contract section velocity [m/s]
C_T	torque coefficient		
C_{TS}	static torque coefficient	<i>Greek</i>	
D	rotor diameter ($D = 2R$) [m]	ϵ	blockage factor
D_{ep}	end plates diameter [m]	λ	tip speed ratio
d	shaft diameter [m]	λ_c	tip speed ratio at which $C_{P,max}$ occurs
H	turbine height [m]	ν	air cinematic viscosity
l	lever arm length [m]	σ	standard deviation
P	power [W]	ω	angular velocity [rad/s]
R	rotor radius [m]	θ	position angle [$^\circ$]
Re	Reynolds number	<i>Subscripts</i>	
		max	maximum value

20 along the support structure (Figure 1). The concept to use different energy sources was derived from the
21 aim to design a standalone system able to have several days of self-sufficiency; i.e. a windy day normally
22 corresponds to a cloudy sky, with low photovoltaic production, and inversely a sunny day corresponds to
23 low wind velocities, with small aeolian production. By combining both energy sources it could be possible
24 to extend the potentiality of a standalone system [1].

25 The choice to use a Savonius wind rotor derives from several positive considerations: it is very simple to
26 realize, economic, compact and has low noise emissions. Besides it works with turbulent and fluctuating wind
27 conditions typical of urban environments, has an high static torque (self starting wind turbine), requires
28 little maintenance and could be easily integrated into design of vertical structures. On the other side the
29 Savonius power performance are lower than three blades horizontal axis wind turbines and so it should be not
30 intended for significant energy production. Many authors have studied the Savonius wind rotor, obtaining
31 maximum power coefficients in the range 0.10 - 0.25. As just mentioned, these are low values if compared to
32 those obtained with other types of wind generators [2, 3]; this reason has led to a large number of numerical
33 and experimental works analysing the factors that could improve the rotor performance. This paper deals
34 again with these topics because of not all variables have been fully investigated and several divergences can
35 be found in literature. Moreover the investigated Savonius rotor was designed to be implemented inside a



Figure 1: The UNIVPM prototype of the experimental street lamp powered by renewable sources.

street lamp and, due to practical constructive choices, different geometric parameters had to be used, some of which not present in literature. For these reasons they were necessary experimental tests in order to evaluate the influence of geometric and constructive parameters on the rotor performance. Experimental measurements were performed in the Environmental Wind Tunnel (EWT) of the UNIVPM. Tests were executed in dynamic conditions on a 1:1 scale model; the rotor twist, the presence of end plates, the effects of blades overlap and the presence of support posts were analysed. Results are illustrated in terms of $C_P - \lambda$ and $C_T - \lambda$ plots for all the different combinations of the tested elements.

2. The Savonius rotor

The selected wind rotor is named Savonius with reference to the Finnish engineer S.J. Savonius, owner of its first patent, which dates back to 1930s [4, 5]. It is a vertical axis wind rotor having a simple geometry. In its most common shape it is made of two semi-cylindrical blades, asymmetrically positioned with respect to the vertical axis of rotation. Motion is generated by unbalanced aerodynamic forces acting on the advancing bucket, which is hit by the flow on its concave side, and the returning bucket, which moves in the opposite direction of the air flow. The concurrent forces system produces a resultant moment along the rotational axis of the rotor, which makes the system rotate. Due to its simple geometry, the Savonius rotor was also used as water turbine with an horizontal axis configuration [6, 7]. According to literature, its geometry can be described by few parameters that are illustrated in Figure 2. Savonius turbine is classified as a drag devices because of the main forces acting on the blades are related to the aerodynamic pressure drag, but a well designed rotor can reach tip speed ratios λ higher than 1.0 (eq. (3)); this result indicates rotational speeds higher than the inlet wind velocity and this is possible only for a rotor also having a lift behaviour.

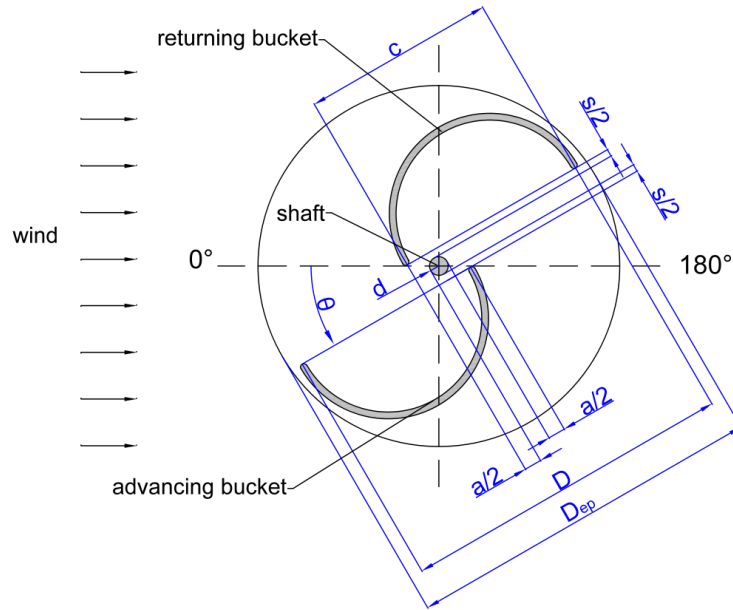


Figure 2: Schematic representation of a classic Savonius rotor section.

56 First investigations, available in literature, have been experimental studies with flow visualizations [8–
 57 11], or experimental tests aimed to measure the average performance of the rotor in terms of static torque
 58 and power coefficient [12]. At a later stage many studies tried to analyse the rotor by measurements of the
 59 surface pressure distribution over a single blade (e.g. [13–18]). In the same period was introduced a first
 60 numerical approach using the discrete vortex method to evaluate the flow field of a Savonius rotor [19–21].
 61 In recent years several authors have used new techniques, as P.I.V. [22] or C.F.D. (e.g. [23–27]), in order to
 62 analyse the fluid dynamic flow field, while others have focused their attention on techniques able to maximize
 63 the rotor performance [6, 28–32].

64 Despite this large number of studies, many authors have reached contrasting conclusions on the role of
 65 the geometrical parameters of the rotor.

66 As example several authors have been positively evaluated the presence of an "open overlap" [12, 17, 18,
 67 21, 33], and have agreed in suggesting an optimum overlap ratio between 10 and 15%. In these conditions
 68 it is possible to observe a jet flow trough the overlap that increases the pressure on the concave side of
 69 the returning blade, thus reducing the overall drag [23]. Conversely other authors negatively evaluate the
 70 presence of open overlap if applied to slightly modified geometries [14, 34].

71 A general agreement can be observed in literature about the periodic behaviour of the torque angular
 72 distribution, with a periodicity equal to the number of rotor blades [34, 35]. Measurements of the static
 73 torque at different rotor angular positions have revealed significant variations; it is possible to observe both
 74 high positive values, that are useful to start the rotor, and negative values, that can give starting problems

75 at certain wind angles. Besides these oscillations may cause unpleasant cyclic stresses to the structure [36].
 76 Such problems can be overcome by employing rotors with an higher number of blades, with staggered stages
 77 [36–39], or alternatively by using blades twisted along their vertical axis. Also in this case there are however
 78 different opinions in literature: as example [40, 41] have observed that the twist or the addition of stages
 79 increase the maximum C_P of the rotor, while others like [35] has measured an opposite result.

80 Likewise the analyses about fluid dynamic parameters have often led to conflicting results: some authors
 81 affirm that the Reynolds number affects both the power coefficient [39, 42] and the static torque coefficient
 82 (C_{TS}) [35], others only C_{TS} [12], still others affirm that it has no influence over the rotor performance
 83 because of they relate differences to the friction of the bearings used in the experimental set-up [14].

84 Further informations about results of experimental analyses performed on these and many other param-
 85 eters can be found in [43], where author offers an extensive and accurate review of the experimental literature
 86 on Savonius rotors.

87 The wind turbine investigated in this work is the "classic" Savonius rotor with circular blades; its geomet-
 88 ric characteristics are illustrated in 3.2. Many authors (e.g. [12, 18, 36, 44]) have suggested, for this kind of
 89 rotor, an optimal configuration which characteristics are shown in Table 1. Several of these parameters have
 90 been adopted for the Savonius rotor tested in this paper, but some were modified (Table 2) in order to:
 91 facilitate the industrial production (as example the choice to use multiple rotor stages rather than twisted
 92 blades), improve the structural stiffness (as example modifying the central shaft diameter and the overlap
 93 ratio) and favour integration inside the lamppost (as example increasing the aspect ratio).

	Optimal solution		
number of buckets	2	helical step	0°/m
overlap ratio (a/c)	10-15 %	shaft presence	no
spacing ratio (s/c)	0	number of stages	2
aspect ratio (H/D)	1-1.2	angle between stages	90°
bucket arc angle	180°	$C_{P,max}$ (1 stage)	≈0.24
end plates D_{ep}/D	1.1	$C_{P,max}$ (2 stages)	≈0.28

Table 1: Optimal configuration for a Savonius rotor with semi-circular blades.

94 3. Experimental apparatus

95 3.1. The Environmental Wind Tunnel (EWT)

96 The EWT is a closed circuit wind tunnel as shown in Figure 3. The test section has a cross square
 97 area of 3.16 m^2 and is subdivided in three main subsections: the former is used for aerodynamic tests that
 98 require a uniform velocity distribution and low turbulence levels. The second one is used to measure the
 99 effects of reciprocal interferences between slender bodies. The latter is the environmental section and is used

100 to test wind effects over buildings, structures and orography models that are immersed into fully developed
 environmental boundary layers. Wind tunnel is equipped with a fan having a constant rotational speed of

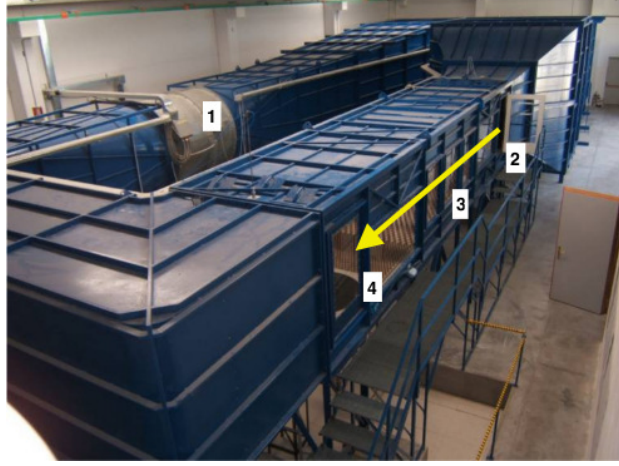


Figure 3: The Environmental Wind Tunnel of the University "Politecnica delle Marche": 1-fan 2-first test subsection 3-second test subsection 4-third test subsection.

101
 102 975 RPM and 16 blades with an adjustable pitch. The average wind speed inside the test section ranges
 103 between 6 m/s and 40 m/s . Measurements carried out with a Constant Temperature Hot Wire Anemometer
 104 (CTA HWA) have shown a 2-D inlet speed uniformity within 2.5% and a turbulence intensity lower than
 105 0.3%. Wind tunnel is also equipped with a compact heat exchanger, that is used to limit temperature
 106 fluctuations within a range of 1 °C.

107 3.2. The rotor models

108 Rotors presented in this research work are Savonius type with semi-circular blades; they are realized in a
 109 1:1 scale with respect to those designed for the street lamp. The models have a diameter D of 0.384 m and
 110 are 1 m high. The section swept by the rotor is therefore of 0.384 m^2 , while the blockage factor, introduced
 111 by [45] and defined in eq. (1), is 3.2 %. Considering also the experimental set-up support structure (fixed
 112 frame), the total blockage area reaches a maximum of 6.1 %. According to eq. (2), introduced in [45], a
 113 correction coefficient was applied to the inlet velocity so to take into account the blockage effect:

$$\epsilon = \frac{A_t}{4S} \quad (1)$$

$$v = v_\infty(1 + \epsilon) \quad (2)$$

114
 115 The rotor is an assembly of modular elements axially connected along a central shaft, having a diameter d
 116 of 37 mm , so to form a "skeleton". Such elements can be aligned or staggered by regular angles with respect
 117 to the vertical axis. In this way it is possible to realize a rotor having a straight or a twisted geometry (i.e.

118 an helical rotor). In this work three rotors have been analysed (Figure 4): two helical rotors with overall
 119 twists respectively of 90° and 105° and a straight rotor (0°). The 105° twist was a technical specification
 120 limit fixed by industrial partners appointed to realize the final prototype. The rotor blades surfaces were
 121 realized with a polyethylene sheet stretched upon the assembled skeleton; this polymeric material allowed
 122 to follow the double curvature given by the twist. The sheet is fixed to the modular ribs and stretched so
 123 as to have a solid and regular surface for the flow. The rotor central shaft and the blades tips are not in
 124 contact and rather they form a gap of 18 mm where the flow can pass through.

125 Referring to Figure 2, the geometric characteristics of the tested rotors are summarized in Table 2.

Adopted solution			
number of buckets	2	helical step	0-90-105°/m
overlap ratio (a/c)	8.2 %	shaft diameter (d)	37 [mm]
spacing ratio (s/c)	0	number of stages	1
aspect ratio (H/D)	2.6	bucket arc angle	180°
end plates D_{ep}/D	no / 1.1	rotor diameter (D)	384 [mm]

Table 2: Geometric parameters of the rotors tested.

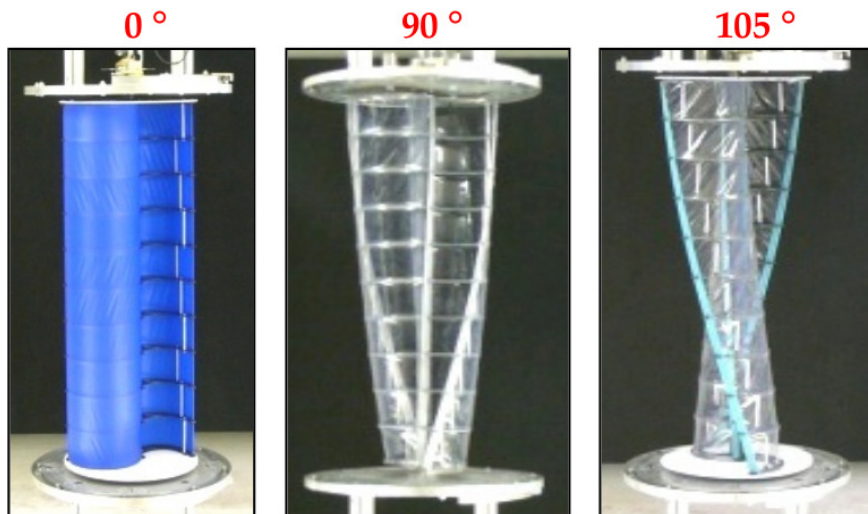


Figure 4: The rotors tested in the present work

126 By comparing these parameters with those in Table 1, it is possible to observe that the design choices
 127 have required a geometry different from the optimal one. Also for this reason it was necessary to perform
 128 an experimental analysis that accurately determines the role of the varied construction parameters: i.e.
 129 end plates, helical step and central gap. Another parameter that was tested is the presence of lamppost
 130 support poles placed externally to the rotor; indeed the street lamp concept provides four steel tubular posts

131 designed to the structural resistance. In this way the helical rotors do not have to support the weight of the
 132 structure and therefore lighter materials can be used.

133 4. The measurements setup and procedure

134 In order to obtain C_P and C_T vs. λ curves for all the tested configurations, both wind speed and rotor
 135 angular velocity should be varied. The wind speed can be changed by adjusting the wind tunnel inlet flow
 136 velocity. The rotor angular velocity is varied by an hydraulic brake that clamps a disk coupled to the rotor
 137 shaft (Figure 5) and changes the counteracting torque; in the real case this action is performed by the torque
 138 of the electric generator coupled to the Savonius rotor. The testing procedure provides the subsequent steps:
 139 first of all a desired wind speed is selected, then the hydraulic brake is modulated on all its braking range,
 140 from null to full. In this way the system stabilises at different equilibrium states between the driving forces
 141 (fluid dynamics actions) and the resistant torque (braking friction loads) and it is possible to obtain enough
 operational points to draw the rotor characteristic curves.

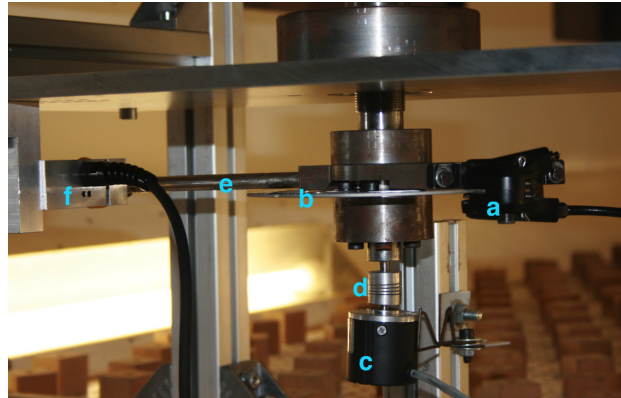


Figure 5: Details of the experimental apparatus: a) brake caliper b) break disk c) encoder d) joint e) lever arm f) load cell

142
 143 Torque and power coefficients C_T and C_P , as also the λ tip speed ratio, are obtained, according to eq. (3)-(4),
 144 by measuring at the same time the torque T and the angular velocity ω .

$$C_T = \frac{T}{0.5 \rho A R v^2} \quad \lambda = \frac{2\pi R \omega}{60 v} \quad (3)$$

$$C_P = \frac{P}{0.5 \rho A v^3} = \lambda C_T \quad (4)$$

146 The measurement apparatus is illustrated in Figure 5. The angular velocity ω is directly acquired as RPMs
 147 by an incremental encoder. A radial lever arm, integrated within the braking system, transmits the torque
 148 T to a mono-axial load cell fixed to the set-up frame. The load cell was calibrated before the tests, using

149 sample weights. The torque is obtained from the simple relationship $T = Fl$, where F is the force measured
 150 on the load cell and l the length of the lever arm.

151 Tests were performed at different inlet flow velocities; a National Instrument data acquisition system was
 152 used for a real-time analysis of the experiment. Data were collected with an acquisition period of 3 seconds
 153 and with a sampling rate of 1024 Hz.

154 5. Evaluation of measurement uncertainties

155 Measured quantities are affected by several sources of uncertainty, that are normally classified as type A
 156 or type B. Type A uncertainties arise from factors that cannot be kept under control or whose effect cannot
 157 be reasonably determined “a priori”. They are usually associated with random fluctuations that occur during
 158 acquisitions. Given a population standard deviation σ of the N values read in single acquisition, the mean
 159 value that can be extracted is subjected to an uncertainty given by eq. (5).

$$160 \quad \sigma_{ave} = \frac{\sigma}{\sqrt{N}} \quad (5)$$

161 Type B uncertainties are those already known or that can be evaluated “a priori” on the basis of the
 162 possible sources of error. In our case they are related to calibration and accuracy of the sensors. Type A
 163 uncertainties were evaluated with the least squares straight line method, while type B uncertainties were
 164 directly derived from the technical specifications of the instruments. When this latter information was not
 165 available, a rectangular error distribution was assumed, which can match the standard deviation of a normal
 166 distribution by dividing the maximum error of the instrument by a factor $\sqrt{3}$. If none of the two types of
 167 error includes the other, the uncertainty of the quantities directly measured is obtained according to eq. (6).
 168 For the derived quantities, the error propagation law was used (7).

$$169 \quad \sigma = \sqrt{\sigma_A^2 + \sigma_B^2} \quad (6)$$

$$170 \quad f = f(x, y) \implies \sigma_f = \sqrt{\left(\frac{\partial f}{\partial x} \sigma_x\right)^2 + \left(\frac{\partial f}{\partial y} \sigma_y\right)^2} \quad (7)$$

171 A 95% confidence level, corresponding to an interval of $\pm 2\sigma$, was chosen in order to evaluate extended
 172 uncertainties. Experimental tests have shown a σ mean value of 2,37% for uncertainties associated with
 173 the single acquisitions, while the error associated with the σ_{ave} average acquisition value is approximately
 174 0,07%.

175 6. Experimental Results

176 Several combinations of the parameters to be investigated were tested in the experimental analyses.
 177 These configurations are summarized in Table 3, where the corresponding reference codes are listed. Each

Test code	Helical step (°/m)	End Plates (E)	Posts (P)
0deg_nE_nP	0	no	no
0deg_yE_nP	0	yes	no
0deg_nE_yP	0	no	yes (4)
0deg_yE_yP	0	yes	yes (4)
90deg_nE_nP	90	no	no
90deg_yE_nP	90	yes	no
90deg_nE_yP	90	no	yes (4)
90deg_yE_yP	90	yes	yes (4)
90deg_yE_yP3	90	yes	yes (3)
105deg_nE_nP	105	no	no
105deg_yE_nP	105	yes	no
105deg_nE_yP	105	no	yes (4)
105deg_yE_yP	105	yes	yes (4)

Table 3: Legend of the main configurations tested.

of the listed configurations was tested in dynamic conditions at different wind velocities v . The T , P vs $\omega(rpm)$ curves as well as the curves of the C_T e C_P vs λ coefficients were extracted.

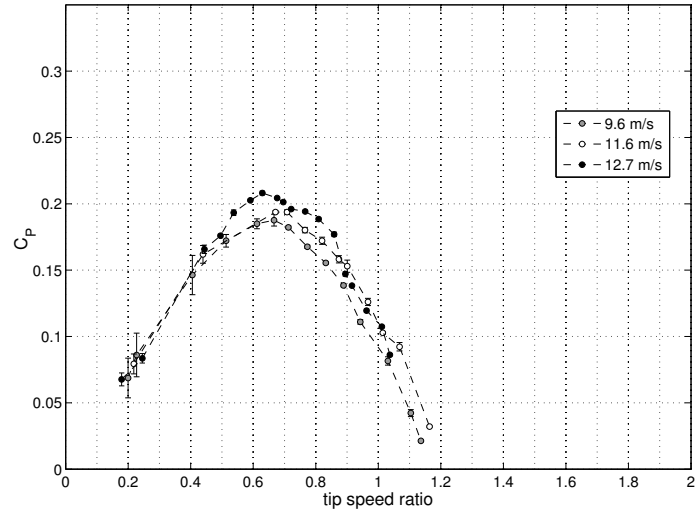
6.1. Effect of the Reynolds number

As previously mentioned, researchers do not agree on the role of the Reynolds number on the performance of Savonius turbines. Some claim a Reynolds number dependency, while other assert that the observed different values of torque and power coefficients, obtained at different Re , are related to the friction of the bearings. Although frictions were not directly measured, a comparison using two different experimental layouts was carried out in this work: the first layout (I) was equipped with small bearings (SKF 4205ATN9, internal diameter 25 mm, external diameter 52 mm, and SKF 6304, internal diameter 20 mm, external diameter 52 mm), the second layout (II) was assembled with considerably oversized bearings (SKF 5306, internal diameter 30 mm, external diameter 72 mm, and SKF 6008, internal diameter 40 mm, external diameter 68 mm). The comparison was made using a rotor with no twist, no end-plates, no posts and with an open overlap (0deg_nE_nP). Results are shown in Figure 6 and Figure 7, while velocities and Reynolds numbers are illustrated in Table 4.

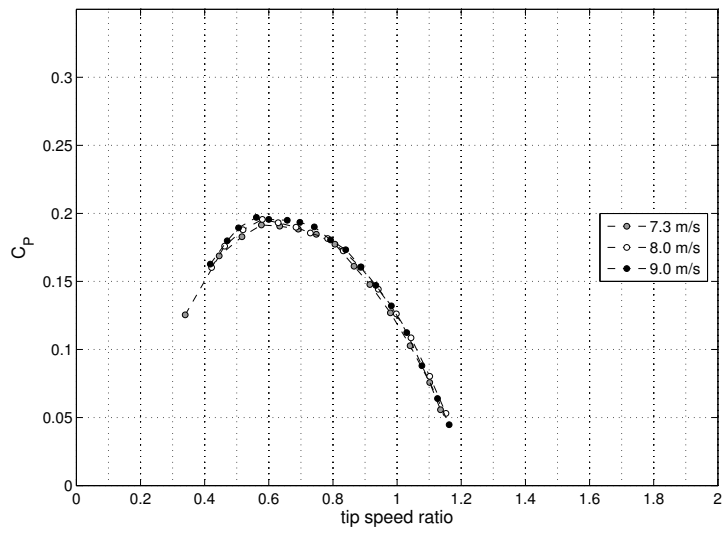
The Reynolds number was calculated according to eq. (8). The dynamic viscosity ν was calculated using the air temperature measured with a properly calibrated RTD PT100.

$$Re = \frac{vD}{\nu} \quad (8)$$

Both tests show identical trends, although the curves carried out with the first assembly (test I) show a small reciprocal divergence at different velocities. Tests with the big bearings (II) was carried out at lower

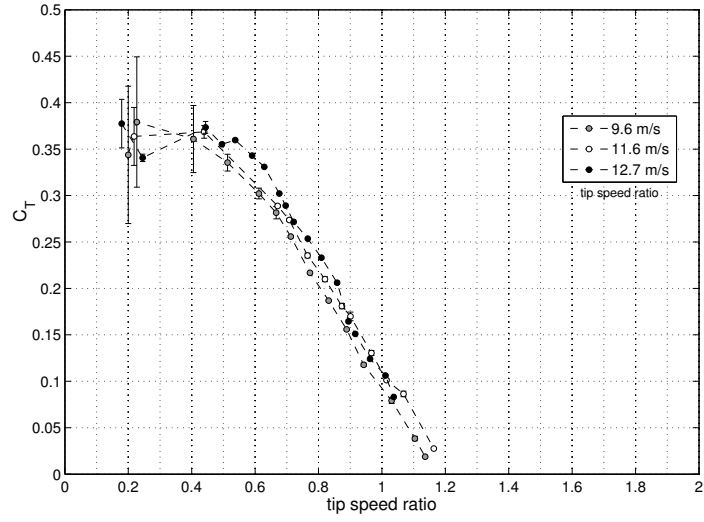


(a) set-up with the small bearings (test I)

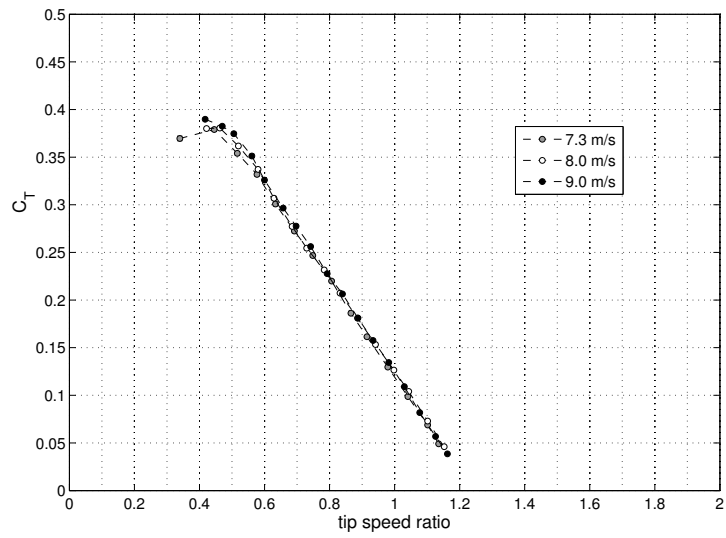


(b) set-up with the big bearings (test II)

Figure 6: Effect of the Re number on the C_P curves.



(a) set-up with the small bearings (test I)



(b) set-up with the big bearings (test II)

Figure 7: Effect of the Re number on the C_T curves.

air speed v_∞	corrected speed v	Re number (I)	Re number (II)
6.9	7.3	–	199'940
7.7	8.1	–	221'851
8.5	9	–	246'501
9.1	9.6	249'629	–
11	11.6	301'635	–
12	12.7	330'238	–

Table 4: Velocities and Re numbers for the tests of Figure 6 and 7.

196 velocities to enhance the relative weight of bearing friction, but the curves perfectly overlap. This indicates
197 that C_P and C_T are independent of the inlet flow selected velocities and, therefore, of the Reynolds number.
198 It is besides plausible to affirm that discrepancies observed in tests with small bearings are due to the
199 greater effects of the mechanical frictions. By regressing the experimental data with a least squares third
200 order polynomial curve is possible to obtain a $C_{P,max} = 0.189$ at $\lambda = 0.67$ for test (I), and a $C_{P,max} = 0.192$
201 at $\lambda = 0.65$ for test (II); i.e. negligible differences.

202 6.2. Effect of the end plates

203 End plates are built in form of circular discs applied to both the ends of the rotor. Their effect is
illustrated in Figure 8 for the straight rotor and in Figure 9(a) and 9(b) for the helical ones.

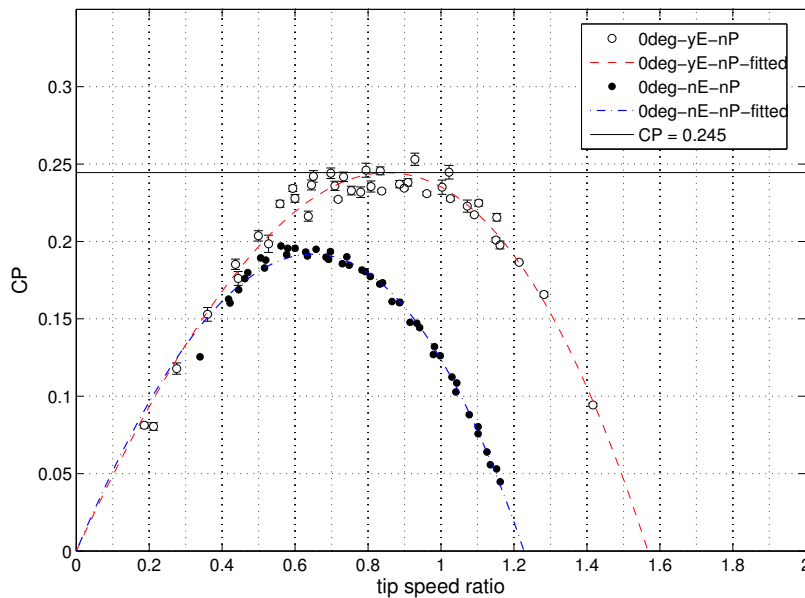
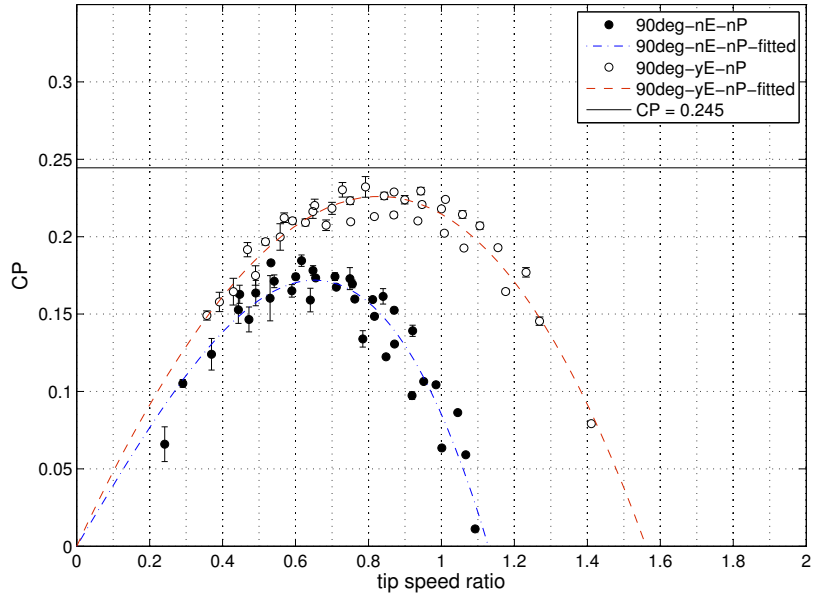
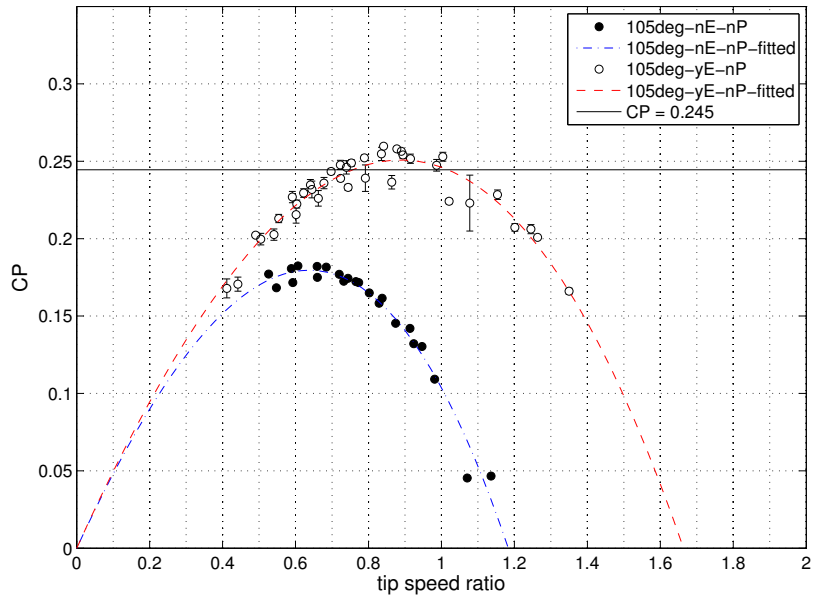


Figure 8: End Plates effect (rotor with no helical step).



(a) Rotor with $90^\circ/m$ helical step.



(b) Rotor with $105^\circ/m$ helical step.

Figure 9: End plates effect on helical rotor efficiency C_P .

204
 205 Graph points refer to the experimental values obtained at different wind velocities, while the fitting curve
 206 was obtained from a least squares third order polynomial regression on all acquired data. An improvement
 207 effect, due to the confinement of the flow inside the rotor, is observable and confirms literature results. In
 208 our case, the improvement of the peak of C_P , as calculated from the fitting curve, is between 27% and 39%;
 209 refer to Table 5. In order to simplify the comparison among the different configurations, an horizontal line,
 210 corresponding to the maximum C_P of a reference test, is shown in the graphs. This reference is the straight
 211 rotor with end-plates (0deg_yE_nP), which corresponds to the most frequent configuration observed in
 literature.

Helical step (°)	0	90	105
whitout End Plates	0.192	0.172	0.18
whit End Plates	0.245	0.226	0.251
variation	+27 %	+31 %	+39 %

Table 5: The $C_{P,max}$ with the presence of End Plates.

212

213 6.3. Effect of the helical step

214 The effect of the helical twist can again be deduced from Table 5, and in Figure 10 the results for the
 215 rotors with end plates are illustrated. It can be noticed that for a configuration with end plates, which
 216 resulted a greater choice, the rotor with a step of 90° has a slightly lower $C_{P,max}$, with respect to a twist
 217 of 105 °; in absence of end plates, the helical step induces lower performance due to the augmented flow
 218 escape.

219 6.4. Effect of the posts

220 The posts are built as vertical cylindrical poles with a diameter of 42 mm and provide a structural
 221 support to the street lamp. They are placed externally at a distance of 635 mm from the center of the
 222 rotor and are arranged at every 90°. Experimental tests were performed with the orientation reported in
 223 Figure 11 in order to evaluate their greatest disturbance effect. Tests were performed by using both three
 224 and four posts. When measuring the configuration with three posts, the one upstream the rotor was removed
 225 (the circle filled with the gray color in Figure 11). Results of these tests are illustrated in Table 6 and in
 226 Figure 12, 13(a) and 13(b); it is possible to observe, as expected, a significant decrease in performance with
 227 four posts and a less evident effect in the case with three posts. This can be explained in two ways:

- 228 - the post upstream the rotor causes disturbance to the incident flow (leeward wake, flow deviation and
 229 overpressure on the incoming blade);
- 230 - the other posts cause only overpressures on the blades approaching them.

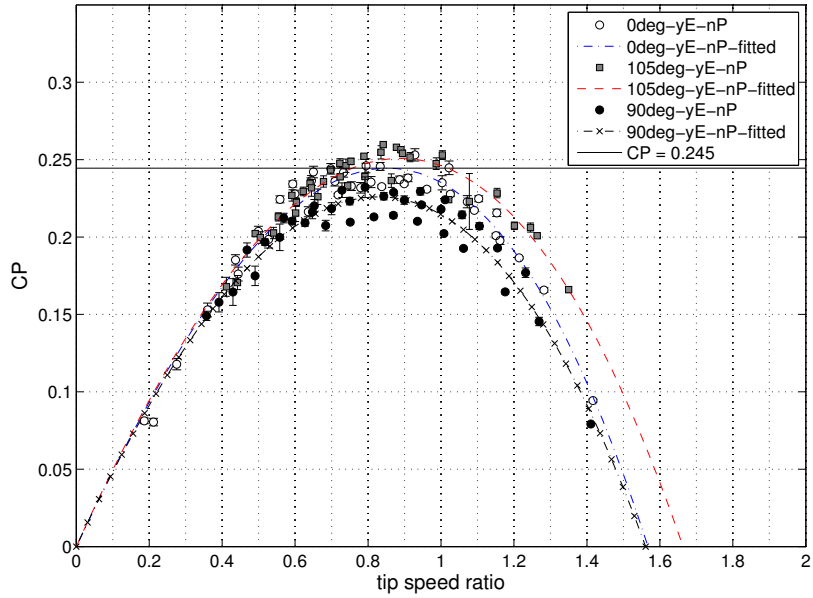


Figure 10: Effect of helical step on rotor efficiency C_P (rotors with End Plates).

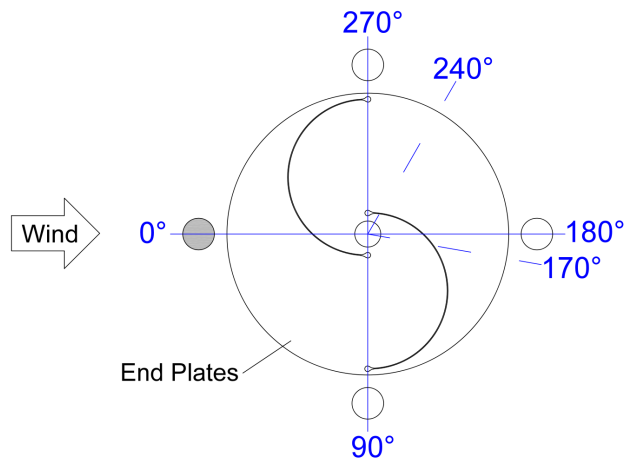


Figure 11: Posts position and used angular references. In tests with three posts the gray element is removed.

231 The last item allows to explain the lesser decrease of performance in test with three posts illustrated in
 232 Figure 12 and Figure 13(a). Finally it can be observed a difference in the effect of the posts depending on
 233 the twist: the rotor twisted by 90° , seems to suffer from this phenomenon more than the others. The better
 234 behaviour was experienced by the 105° due to the phase shift among the blade sections approaching to the
 post.

Posts	Helical step ($^\circ/\text{m}$)		
	0	90	105
no	0.245	0.226	0.251
3 posts	0.224 (-8.2 %)	0.195 (-13.7 %)	—
4 posts	0.187 (-23.4 %)	0.155 (-31.4 %)	0.206 (-17.9 %)

Table 6: $C_{P,max}$ with the presence of posts.

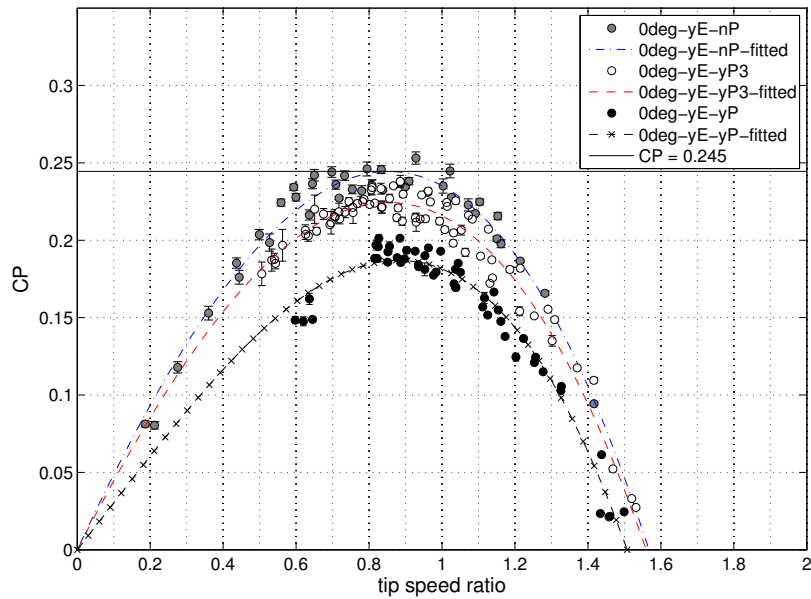
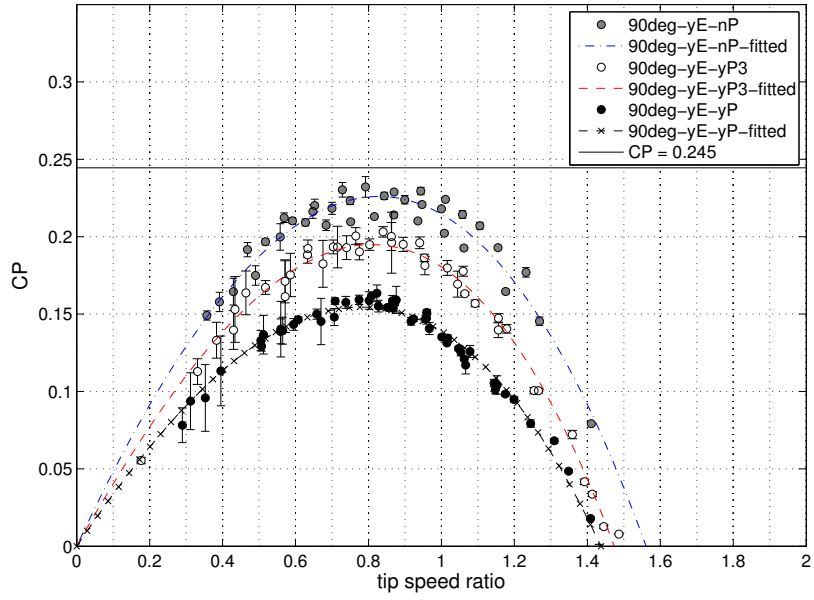


Figure 12: Effect of the posts on the rotor efficiency C_P .

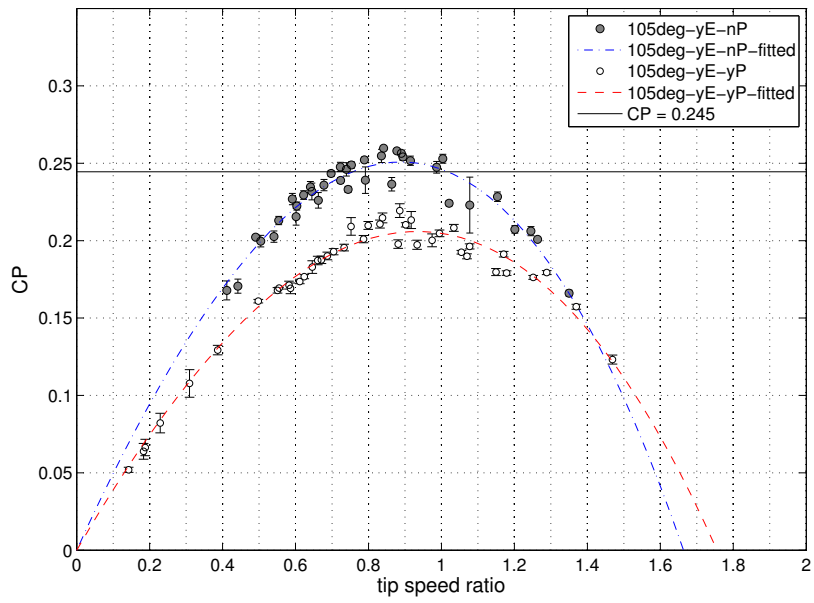
235

236 6.5. External grid effect

237 An issue, that came out in the street lamp design process, was to test some systems to protect the
 238 rotating parts from collisions with external objects. A simple solution is a wire mesh to be placed externally
 239 to the wind rotors. These grids provide an adequate mechanical protection but they also induce pressure
 240 drops in the flow: this could negatively affect the performance of the wind rotor by reducing the available
 241 wind dynamic pressure to be converted. In order to evaluate such effects, different configurations were tested



(a) Rotor with 90°helical step.



(b) Rotor with 105°helical step.

Figure 13: Effect of the posts on the helical rotor efficiency C_P .

242 using two different wire meshes with square openings: the former has a square side length of 1 cm (normal
 243 grid), the latter has a side of 6 cm (wider and lighter grid). The ratio between the total area and the
 244 mesh open area, defined as porosity, is of the 70% in the first case and 95% in the second one. Tests were
 245 performed on the 105° helical rotor without end plates and results are shown in Figure 14. Experiments
 246 have showed that rotor performance strongly decrease (-32 % on $C_{P,max}$) by placing a normal grid on the
 247 whole rotor circumference (black circles). So a gradual increase of the porosity was performed by lightening
 248 the normal grid in different positions (see Figure 14):

- 249 - in the frontal zone (LGA, white circles);
- 250 - in the frontal and in the back zone (LGab, white triangles);
- 251 - in the advancing bucket side (LGc, blue triangles);
- 252 - in the most part of the rotor (LGd, red square).

253 Finally a last configuration without any grid in the advancing bucket side (black square) was tested. Results
 254 show that all adopted solutions reduce rotor performance in a similar way but the worst solution is the
 configuration with the normal grid (black circles). The main numerical results are reported in Table 7.

Code	Light grid (LG)	Normal grid (G)	$C_{P,max}$
105deg_nE_nP	no	no	0.18
105deg_nE_yG	no	0°-360°	-32 %
105deg_nE_yG_LGa	0°-90°	elsewhere	-23 %
105deg_nE_yG_LGab	0°-90°, 170°-240°	elsewhere	-21 %
105deg_nE_yG_LGc	0°-180°	elsewhere	-18 %
105deg_nE_yG_LGd	0°-240°	elsewhere	-14 %
105deg_nE_yG180	no	180°-360°	-14 %

Table 7: Variation of the $C_{P,max}$ with the presence of external grid (see also Figure 11).

255

256 6.6. Effect of the overlap

257 The influence of the overlap was examined by closing the gap near the rotational axis with an insulating
 258 tape. The helical rotor with a twist of 105° was used to analyse the jet-flow effect. Results illustrated in
 259 Figure 15 show that the absence of the gap causes a decrease of $C_{P,max}$ by 17%.

260 7. Concluding remarks

261 This article reports the results of experimental tests performed in a wind tunnel on a Savonius wind rotor
 262 to be used on a street lamp powered by renewable energy. Practical design requirements and architectural
 263 restrictions impose some not optimal choices about the Savonius geometry as compared with scientific
 264 literature (as example an higher aspect ratio); this forces authors to carry out new experimental analyses

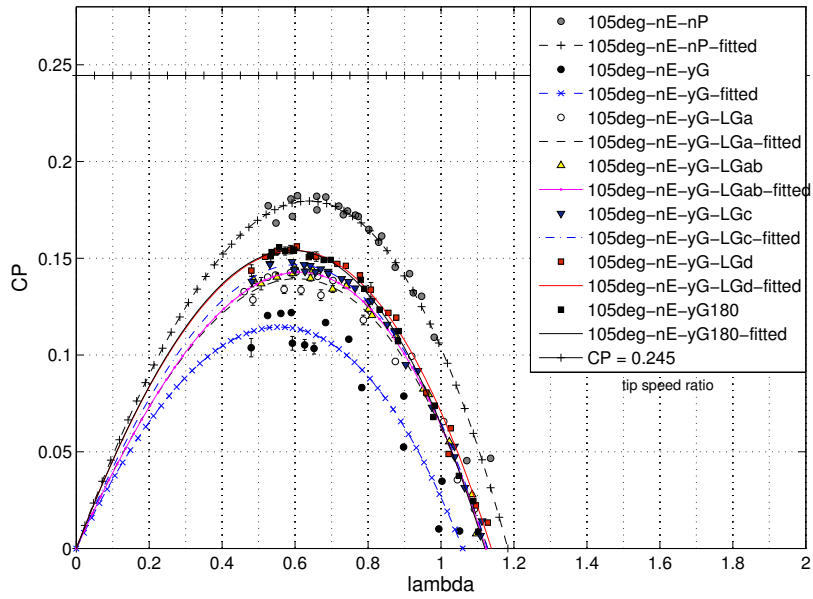


Figure 14: Grid effect (rotor with 105°h.s., no End Plates).

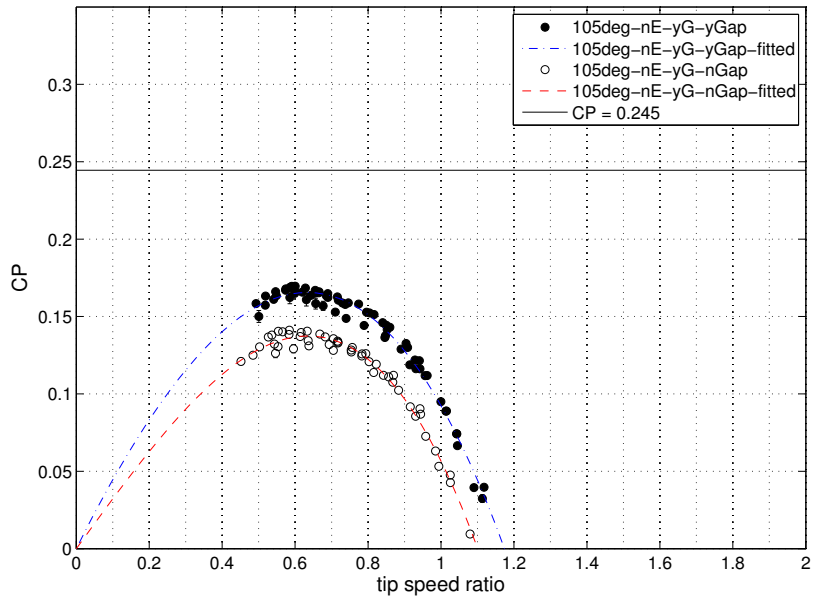


Figure 15: Open overlap effect (rotor with 105°h.s. and grid).

265 in order to redefine new optimal configurations and verify performance. Tests were carried out to evaluate
 266 the influence on the rotor performance of single or combined applications of: Reynolds number, helical step
 267 of 0, 90 and 105°, open overlap, end plates and external pillar posts. The overall results of the performed
 tests are shown in Table 8.

Test code	Helical Step (°/m)	End Plates (E)	Posts (P)	Light grid (LG)	Normal grid (G)	$C_{P,max}$	λ_C	λ_{max}
0deg_nE_nP	0	no	no	no	no	0.192	0.649	1.16
0deg_yE_nP	0	yes	no	no	no	0.245	0.854	1.57
0deg_yE_yP	0	yes	yes (4)	no	no	0.187	0.882	1.51
0deg_yE_yP3	0	yes	yes (3)	no	no	0.224	0.853	1.56
90deg_nE_nP	90	no	no	no	no	0.172	0.652	1.13
90deg_yE_nP	90	yes	no	no	no	0.226	0.828	1.56
90deg_yE_yP	90	yes	yes (4)	no	no	0.155	0.781	1.44
90deg_yE_yP3	90	yes	yes (3)	no	no	0.195	0.809	1.47
105deg_nE_nP	105	no	no	no	no	0.180	0.637	1.18
105deg_yE_nP	105	yes	no	no	no	0.251	0.889	1.66
105deg_yE_yP	105	yes	yes (4)	no	no	0.206	0.934	1.76
105deg_nE_yG	105	yes	yes	no	0-360°	0.122	0.597	1.07
105deg_nE_yG_LGa	105	yes	yes	0-90°	elsewhere	0.139	0.605	1.13
105deg_nE_yG_LGab	105	yes	yes	0-90+170-240°	elsewhere	0.143	0.612	1.13
105deg_nE_yG_LGc	105	yes	yes	0-180°	elsewhere	0.147	0.603	1.13
105deg_nE_yG_LGd	105	yes	yes	0-240°	elsewhere	0.154	0.597	1.14
105deg_nE_yG180	105	yes	yes	no	180-360°	0.154	0.590	1.12

Table 8: Summary of main experimental results.

268

269

The main findings of this study are instead hereinafter summarized:

270

- The tests were performed for Reynolds numbers between 200000 and 330000: in this range the performance (C_P e C_T) were not dependent on the Reynolds number;

271

- The absence of the open overlap causes a decrease in the performance on $C_{P,max}$ of about 17%;

272

- The helical rotor has lower performance than the straight rotor if the step is of 90°, (-6/7% on $C_{P,max}$), while a twist of 105 ° shows similar performance;

273

- The end plates always have an improving effect, which however is greater for the helical rotor with a step of 105°, (+ 39% on $C_{P,max}$);

274

- The supporting posts negatively affect the performance due to two reasons:

275

a) leeward wake;

276

b) overpressure generated on the approaching blade;

277

- The negative effect of the posts, which can reach - 31.4% of $C_{P,max}$, is not the same for all rotors: the

278

279

280

281 effect is smaller for an helical rotor with a step of 105° , (-17.9%);
 282 • External grids have a negative effect on the rotor performance depending on the grid position and
 283 porosity.
 284 • Best results were obtained for an helical rotor with a step of 105° , with end plates and open gap; in
 285 this conditions a $C_{P,max}$ of 0.251 at $\lambda = 0.899$ was measured.

286 8. Acknowledgments

287 This work was realized thanks to the support of the projects IPA P.O.W.E.R.E.D and Ministry of
 288 Economic Development INDUSTRIA 2015 (www.powered-ipa.it).

289 9. References

- 290 [1] R. Ricci, S. Montelpare, D. Vitali, An innovative wind-solar hybrid street light: development and early testing of a
 291 prototype, *International Journal of Low-Carbon Technologies* 0 (2014) 1–10.
- 292 [2] R. E. Wilson, P. B. Lissaman, *Applied Aerodynamics of wind power machines*, no. GI-41840 in *Research Applied to*
 293 *National Needs*, Oregon State University, 1974.
- 294 [3] A. Jha, *Wind Turbine Technology*, ISBN 13: 978-1-4398-1507-6, CRC Press, 2011.
- 295 [4] S. J. Savonius, The S-rotor and its applications, *Mechanical Engineering* 5 (53) (1931) 333–338.
- 296 [5] S. J. Savonius, *The wing rotor in theory and practice*, Savonius Co., 1928.
- 297 [6] K. Golecha, T. Eldho, S. Prabhu, Influence of the deflector plate on the performance of modified Savonius water turbine,
 298 *Applied Energy* (88) (2011) 3207–3217.
- 299 [7] M. Khan, G. Bhuyan, M. Iqbal, J. Quaicoe, Hydrokinetic energy conversion systems and assessment of horizontal and
 300 vertical axis turbines for river and tidal applications: A technology status review, *Applied Energy* (86) (2009) 1823–1835.
- 301 [8] G. von Bach, Untersuchungen fiber Savonius-rotoren und verwandte strömungsmaschinen, *Forsh. Geb. Ing.* 2 (1931)
 302 218–231.
- 303 [9] G. Bergeles, N. Athanassiadis, On the flow field around a Savonius rotor, *Wind Eng.* 6 (1982) 140–148.
- 304 [10] G. J. Bowden, S. A. McAleese, The properties of isolated and coupled Savonius rotors, *Wind Eng.* 8 (1984) 271–288.
- 305 [11] J. Massons, J. Gavalda, X. Ruiz, F. Diaz, Image analysis of the wake generated by a Savonius rotor, *Wind Eng.* 12 (1988)
 306 341–351.
- 307 [12] B. F. Blackwell, R. E. Sheldahl, L. V. Feltz, Wind tunnel performance data for two and three bucket Savonius rotors,
 308 United States Energy Research and Development Administration under contract AT .
- 309 [13] A. Chauvin, D. Benghrib, Drag and lift coefficients evolution of a Savonius rotor, *Experiments in Fluids* 8 (1989) 118–120.
- 310 [14] V. J. Modi, M. S. U. K. Fernando, On the performance of the Savonius wind turbine, *Journal of Solar Energy Engineering*
 311 111 (1989) 71–81.
- 312 [15] V. J. Modi, M. S. U. K. Fernando, N. J. Roth, *Aerodynamics of the savonius rotor: experiments and analysis*, vol. 5,
 313 IECEC, Energy Conversion Engineering Conference. Proceedings of the 25th Intersociety, 213 – 218, 1990.
- 314 [16] M. Kotb, T. Aldoss, Flowfield around a partially-blocked Savonius rotor, *Applied Energy* 38 (2) (1991) 17–132.
- 315 [17] N. Fujisawa, F. Gotoh, Visualization study of the flow in and around a Savonius rotor, *Experiments in Fluids* (12) (1992)
 316 407–412.
- 317 [18] N. Fujisawa, On the torque mechanism of Savonius rotors, *Journal of Wind Engineering and Industrial Aerodynamics* 40
 318 (1992) 277–292.

- 319 [19] M. S. U. K. Fernando, V. J. Modi, A numerical analysis of the unsteady flow past a Savonius wind turbine, *Journal of*
320 *Wind Engineering and Industrial Aerodynamics* (32) (1989) 303–327.
- 321 [20] V. J. Modi, M. S. U. K. Fernando, Unsteady aerodynamics and wake of the Savonius wind turbine: a numerical study,
322 *Journal of Wind Engineering and Industrial Aerodynamics* 46-47 (1993) 811–816.
- 323 [21] N. Fujisawa, Velocity measurements and numerical calculations of flow fields in and around Savonius rotors, *Journal of*
324 *Wind Engineering and Industrial Aerodynamics* 59 (1996) 39–50.
- 325 [22] A. Shigetomi, Y. Murai, Y. Tasaka, Y. Takeda, Interactive flow field around two Savonius turbines, *Renewable Energy*
326 (2011) 536–545.
- 327 [23] V. D’Alessandro, S. Montelpare, R. Ricci, A. Secchiaroli, Unsteady Aerodynamics of a Savonius wind rotor: a new
328 computational approach for the simulation of energy performance, *Energy* 35 (8) (2010) 3349–3363.
- 329 [24] S. Roy, U. K. Saha, Review on the numerical investigations into the design and development of Savonius wind rotors,
330 *Renewable and Sustainable Energy Reviews* (23) (2013) 73–83.
- 331 [25] K. Kacprzak, G. Liskiewicz, K. Sobczak, Numerical investigation of conventional and modified Savonius wind turbines,
332 *Renewable Energy* (60) (2013) 578–585.
- 333 [26] L. A. Danao, J. Edwards, O. Eboibi, R. Howell, A numerical investigation into the influence of unsteady wind on the
334 performance and aerodynamics of a vertical axis wind turbine, *Applied Energy* (116) (2014) 111–124.
- 335 [27] M. Tartuferi, V. D’Alessandro, S. Montelpare, R. Ricci, Enhancement of Savonius wind rotor aerodynamic performance:
336 a computational study of new blade shapes and curtain systems, *Energy* 79 (2015) 371–384.
- 337 [28] B. M. Shaughnessy, S. D. Probert, Partially-blocked savonius rotor, *Applied Energy* (43) (1992) 239–249.
- 338 [29] I. Dobrev, F. Massouh, CFD and PIV investigation of unsteady flow through Savonius wind turbine, *Energy Procedia*
339 (2011) 711–720.
- 340 [30] B. Altan, M. Atilgan, The use of a curtain design to increase the performance level of a Savonius wind rotors, *Renewable*
341 *Energy* 35 (4) (2010) 821–829.
- 342 [31] S. Rolland, M. Thatcher, W. Newton, A. Williams, T. Croft, D. Gethin, M. Cross, Benchmark experiments for simulations
343 of a vertical axis wind turbine, *Applied Energy* (111) (2013) 1183–1194.
- 344 [32] S. Roy, U. K. Saha, Wind tunnel experiments of a newly developed two-bladed Savonius-style wind turbine, *Applied*
345 *Energy* 137 (2015) 117–125.
- 346 [33] R. Ricci, S. Montelpare, G. Borrelli, V. D’Alessandro, Experimental Analysis of a Savonius Wind Rotor for Streetlighting
347 Systems, in: *Thermal and Environmental issue in energy systems*, Sorrento, Italy, 603–607, 2010.
- 348 [34] M. A. Kamoji, S. B. Kedare, S. V. Prabhu, Experimental investigations on single stage modified Savonius rotor, *Applied*
349 *Energy* 86 (7-8) (2009) 1064–1073.
- 350 [35] M. Kamoji, S. Kedare, S. Prabhu, Performance tests on helical Savonius rotors, *Renewable Energy* 34 (3) (2009) 521–529.
- 351 [36] T. Hayashi, Y. LI, Y. Hara, Wind tunnel tests on a different phase three-stage Savonius rotor, *JSME International Journal*
352 48 (1, series B).
- 353 [37] J. L. Menet, A double-step Savonius rotor for local production of electricity: a design study, *Renewable Energy* 29 (11)
354 (2004) 1843–1862.
- 355 [38] N. Mahmoud, El-Haroun, E. Wahba, M. Nasef, An experimental study on improvement of Savonius rotor performance,
356 *Alexandria Engineering Journal* (51) (2012) 19–25.
- 357 [39] J. Kumburnuss, J. Chen, H. Yang, L. Lu, Investigation into the relationship of the overlap ratio and shift angle of
358 double stage three bladed vertical axis wind turbine (VAWT), *Journal of Wind Engineering and Industrial Aerodynamics*
359 (107-108) (2012) 57–75.
- 360 [40] U. K. Saha, M. Rajkumar, On the performance analysis of Savonius rotor with twisted blades, *Renewable Energy* 31 (11)
361 (2006) 1776–1788.

- 362 [41] U. K. Saha, S. Thotla, D. Maity, Optimum design configuration of Savonius rotor through wind tunnel experiments,
363 Journal of Wind Engineering and Industrial Aerodynamics 96 (8-9) (2008) 1359–1375.
- 364 [42] A. Damak, Z. Driss, M. Abid, Experimental investigation of helical Savonius rotor with a twist of 180° , Renewable Energy
365 (52) (2013) 136–142.
- 366 [43] J. V. Akwa, H. A. Vielmo, A. P. Petry, A review on the performance of Savonius wind turbines, Renewable and Sustainable
367 Energy Reviews 16 (5) (2012) 3054 – 3064, ISSN 1364-0321.
- 368 [44] M. Nakajima, S. Iio, T. Ikeda, Performance of double-step Savonius rotor for environmentally friendly hydraulic turbine,
369 Journal of Fluid Science and Technology 3 (3) (2008) 410–419.
- 370 [45] A. Pope, J. B. Barlow, W. H. Rae, Low-Speed Wind Tunnel Testing, John Wiley & Sons, 3rd edn., 1999.